2D $Ge_2Sb_2Te_5$ phase change material

Bo Zhang[a], Veronika Cicmancova[b], Jaroslav Kupcik[c], Slang Stanislav[b], Roman Svoboda[d], Petr Kutalek[e], Tomas Wagner[a, b]

[a.] *Department of General and Inorganic Chemistry, Faculty of Chemical Technology, University of Pardubice, Studentska 573, 532 10 Pardubice, Czech Republic*
[b.] *Center of Materials and Nanotechnologies, Faculty of Chemical Technology, University of Pardubice, Nam. Cs. Legii 565, 530 02 Pardubice, Czech Republic*
[c.] *Institute of Inorganic Chemistry, ASCR, 250 68 Husinec-Řež Czech Republic.*
[d.] *Department of Physical Chemistry Faculty of Chemical Technology, University of Pardubice, Studentska 573, 532 10 Pardubice, Czech Republic*
[e.] *Joint Laboratory of Solid State Chemistry, University of Pardubice, Studentska 84, 532 10 Pardubice, Czech Republic*

Introduction

Phase change memory is one of the most prominent research fields, since the microchip, for instance 3D Xpoint, has been released in the market [1]. Generally, a phase change material must comprise of at least two solid phases, including crystal or amorphous phases [2]. The optical or electric properties between different phases are often very different [3]. Therefore, the data can be stored into the materials, if the transition between each phase are fast enough [4]. The heating is believed to be the motivation of phase change, where includes of optical heating and electric Joule heating [5,6].

Although multiple different chalcogenide compounds were studied in recent years [7], the traditional compound in PCRAM (Phase-change memory) is Ge-Sb-Te system (GST) [8]. In order to induce crystallization, the amorphous GST film has to be heated to the crystallization temperature in certain duration before cooling down. On contrary, the formation of amorphous phase needs higher temperature and short pulse duration, which the GST film has to be heated above melting temperature and rapidly quenched. Specifically, the length of pulse duration can be as short as 10 ns in amorphous phase and 50 ns in crystallization phase with laser pulses [9].

However, the phase change mechanism is still not fully understood [10]. Several studies including mathematical modelling, for instance ab initio molecular dynamic simulation, were applied to explore phase change transformation [11]. In $Ge_2Sb_2Te_5$ (GST 225) material, amorphous GST film owns high electrical resistivity which can be switched to two low resistivity states (cubic and hexagonal state) [12]. From point of microchip, the GST material is switched between amorphous and crystalline states via electrically induced Joule heat [1314]. However, electrical conductivity of crystalline GST thin film shows many intermediate states, which lie between set and reset values of resistivity. A mixed phase model is put forward to explain the differences. Specifically, overall electrical conductivity is influenced by high and low resistive states [15,16].

Chalcogenides are well known also as the TMDs (Transition metal dichalcogenides). It is one of the most important 2D material groups. The layered TMDs have the generic formula MX_2, where M stands for a metal and X represents a chalcogen. The layered TMDs are investigated in the application of catalysis, gas sensing and optoelectronic devices [17,18,19].

In our paper, we found as-deposited GST 225 thin film prepared by magnetron sputtering contains stacks of 2D monolayers. Furthermore, after exfoliation, amorphous or crystalline 2D flakes are also obtained. The 2D structural model of phase change material is useful for designing microchip and for developing of a new type of electronic devices in the future. Finally, we have to clarify the concept of term “phase change”. In 2D material study, the intercalation of metals leads to the phase transformation, for instance Li intercalation in 2H-MoS_2 [20]. In this paper, the phase transformation means the amorphous-crystalline phase transformation and exfoliation is managed by acetone molecules.

Results and discussion

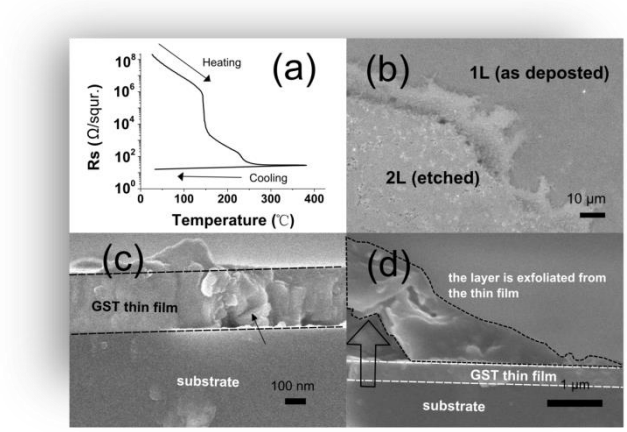

Figure 1 (a)Van der Pauw sheet resistance measured on GST film during heating scan at a rate 2℃/min. (b) The SEM image of amorphous GST thin film after the acetone exfoliation. Two monolayers are marked. (c) The cross sectional view of amorphous GST thin film. (d) The cross sectional view of amorphous GST thin film after acetone exfoliation. The layer (in dashed line area) is exfoliated from the thin film.

The crystallization process of amorphous GST film was detected by the Van der Pauw method (Figure 1 (a)). According to the sheet resistance, the GST thin film initiates the crystallization at the crystallization temperature T_{c1} = at 150℃. During this step, the amorphous material crystallizes to cubic phase [12]. Then with further increase of temperature, the GST material starts to form hexagonal phase at T_{c2} = 250℃ [12]. As the hexagonal phase GST thin film has the lowest resistance, the GST crystalline samples in our paper are annealed at 270℃ (referred as crystalline GST thin film or flakes). The SEM image of amorphous GST film is presented in Figure 1 (b), where part of the GST thin film is exfoliated by acetone. And the observation angle of Figure 1 (b) is shown as 3 in Figure S1. In the lighter part, the topmost amorphous 2D monolayers are exfoliated and dispersed into the acetone solution. It manifests the amorphous GST thin film is in layered structure after deposition. However, the 2D monolayer can not be observed from the side view of amorphous as-deposited GST film, where the GST thin film structure is compact (Figure 1(c)). There is just visible column structure, pointed by the black arrow. However, after acetone exfoliation, layers can be exfoliated from the GST thin film, as shown in Figure 1 (d). The observation angle of Figure 1 (c) and (d) is shown as 5, shown in Figure S1.

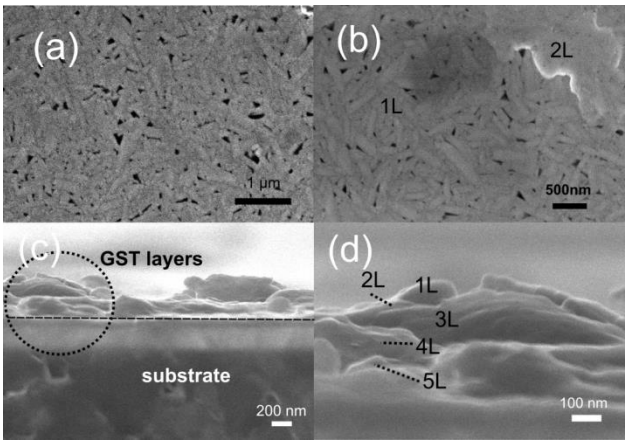

Figure 2 (a) The SEM image of crystallized GST thin film. (b) The SEM image of crystallized GST thin film with two monolayers. (c) The cross sectional view of crystallized GST thin film. (d) The enlarged image of the dashed line circle in Figure (c), where 5 monolayers are marked (1L-5L).

The amorphous GST layer has been transformed to crystalline phase after annealing at the temperature 270℃. Figure 2 (a) shows the surface morphology of the crystalline GST film (observation angle 3 in Figure S1). Some structural evidences can be seen, such as the crystalline grains. In our opinion, the 2D monolayers are partially exfoliated after heating. Figure 2 (b) shows two monolayers at the surface of crystalline GST thin film (observation angle 3 in Figure S1). The topmost monolayer (monolayer 1) is exfoliated and partially removed by the blowing of compressed gas. The cross sectional view of crystalline GST thin film gives further evidence of the layered structure (observation angle 1 in Figure S1). The layers are clearly visible

in Figure 2 (c). At least 5 monolayers are marked in Figure 2 (d) and in comparison with Figure 1 (c), the layered structure appears after crystallization. More examples of layered structure can be found in Figure S2.

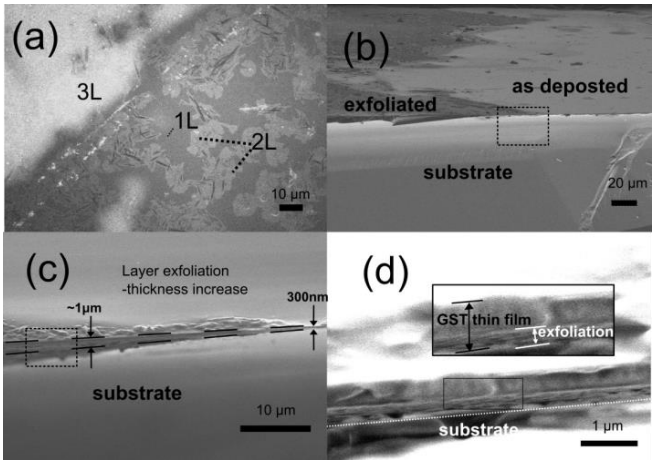

Figure 3.(a) The SEM image of crystallized GST thin film exfoliated by acetone. (b) The side view of crystalline GST thin film at the boundary between exfoliated region and region without contact with acetone. (c) The enlarged region of dashed square in Figure (b). (d) The cross section of GST thin film is the further enlarged dashed square in Figure (c), where the exfoliated part is seen.

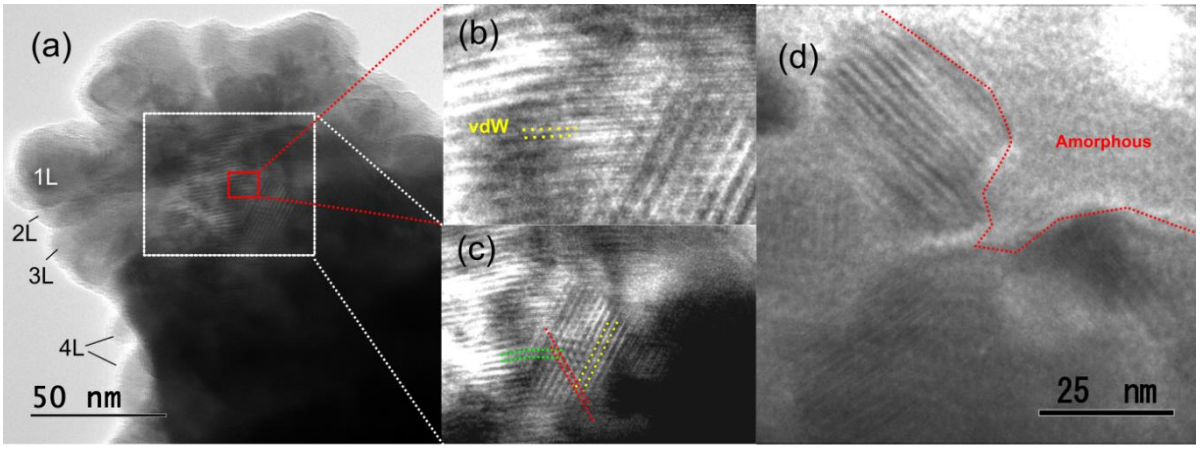

Figure 4 (a) The HRTEM (High Resolution transmission Electron Microscopy) image of layered crystalline GST thin film, where 4 monolayers are identified from the edge of sample. (b) The enlarged image of the dashed square in Figure (a), where Van der Waals gap is marked with yellow dash line. (c) The enlarged image of the dashed square in Figure (a), where different crystalline orientations are recognized via the Van der Waals gaps. (d) HRTEM images of the boundary between crystalline and amorphous phase on the very edge of the sample.

Although the crystalline GST thin film is partially exfoliated, acetone exfoliation is still necessary. Figure 3 (a) shows the surface morphology of crystalline GST thin film after acetone exfoliation, where some GST monolayers are dispersed in the acetone solution and acetone with flakes is removed afterwards (observation angle 3 in Figure S1). Three monolayers are identified from the contrast differences. The SEM image shows the cross sectional view of the exfoliated crystalline GST thin film (Figure 3 (b)-(d)) (observation angle 2 in Figure S1). Between the exfoliated part and the part without contact with acetone, we can see a clear boundary In Figure 3 (b). At the boundary, Figure 3 (c) shows a thickness increase from 300 nm to ~1 μm after exfoliation. In Figure 3 (d), we can see the overall thickness of thin film is increased by the exfoliation. In summary, the overall exfoliation is a two-step process. Firstly, the GST thin film is partially exfoliated during crystallization and further exfoliated with the assistance of acetone.

The sample of crystallized GST thin film in Figure 4 (a) was mechanically separated from the substrate. According to the edge of sample, we can identify at least 4 monolayers. In the middle part of the image (Figure 4 (b)), the crystal structure is seen clearly. The diffraction pattern shows the GST crystal in hexagonal phase (details in Figure S3. supplementary material) where Van der Waals gap is marked with the yellow dotted line [21, 22, 23 ,24]. Based on presence of the Van der Waals gaps, different crystalline orientations are recognized. In some other cases, especially at the edge of thin film, the 2D monolayer has amorphous structure in Figure 4 (d). The EDX (Energy-dispersive X-ray spectroscopy) spectra are shown in Figure S4.

The EDX analysis shows similar composition of as deposited thin film ($Ge_{2.1}Sb_{2.1}Te_{5.7}$) to the target composition $Ge_2Sb_2Te_5$. After crystallization, the composition changes to $Ge_2Sb_{2.1}Te_{4.8}$. The content of Te is slightly reduced.

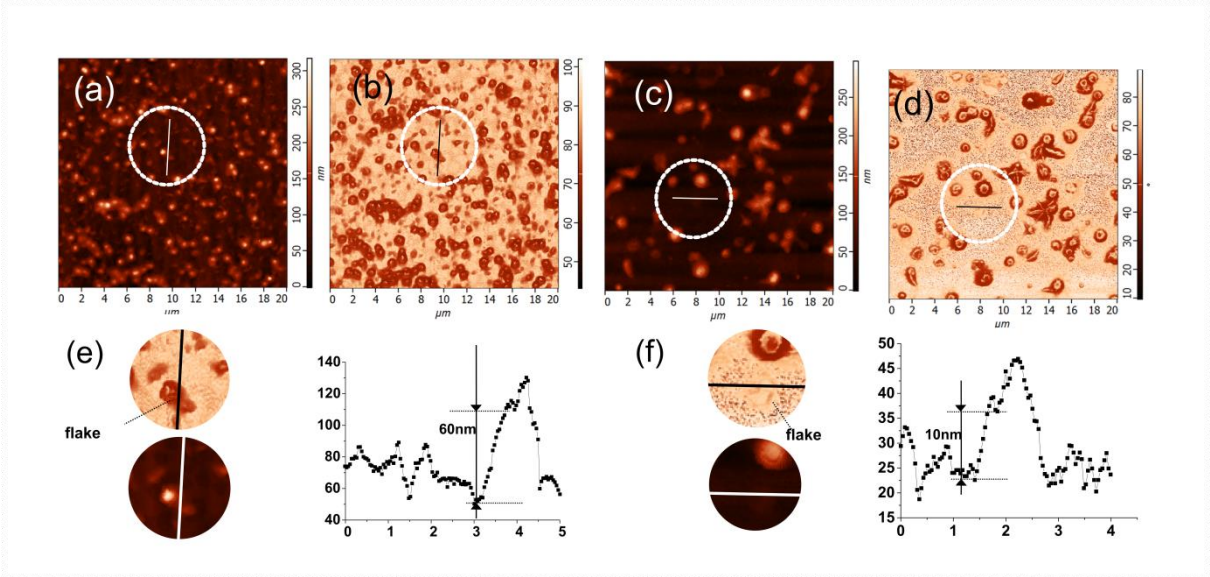

Figure 5 (a) The AFM topography of amorphous GST flakes. (b) The phase image of Figure (a). (c) The AFM topography of crystalline GST flakes. (d) The phase image of Figure (c). (e) The profile is taken from the line scan in Figure (a) (in white circle). The regions in Figure (a) and (b) (white circle) are enlarged on the left side. (f) The profile taken from the line scan in Figure (c). The regions in Figure (c) and (d) (white circle) are enlarged on the left side.

The crystalline GST thin film, no matter amorphous or crystalline, comprises a layered structure. After acetone exfoliation, the flakes are removed from GST thin film. The flakes are transferred to a silicon substrate with tungsten thin film and are observed via AFM and SEM. In Figure 5, two types of AFM images are presented: the topography image and phase image. By comparison of two images, the phase image has better resolution to recognize the boundary of flakes. According to the phase images, the profiles of flakes are taken at the place of lines (marked by the white circle). Generally, the size of flakes from crystalline GST thin film is larger than those from amorphous GST thin film. Moreover, the thickness of crystalline flake can be much thinner (10 nm) in Figure 5 (f) than amorphous flake (60 nm) in Figure 5 (e). Moreover, the flakes shown in Figure 5 (e) and (f) have two 2D monolayers. The SEM image gives more details of the flakes (Figure S5).

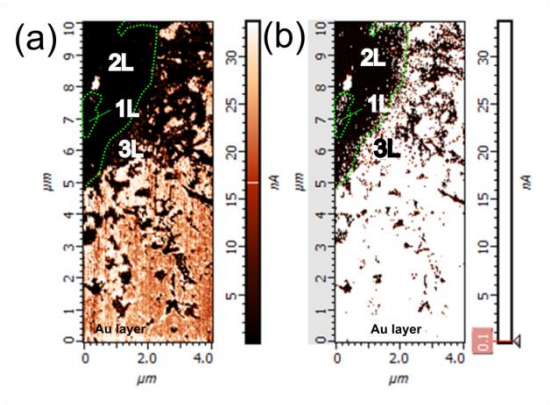

Figure 6 The electrical property of crystalline flakes, measured by conductive AFM. (a)-(b) The current distribution of the crystalline GST flakes in different scales.

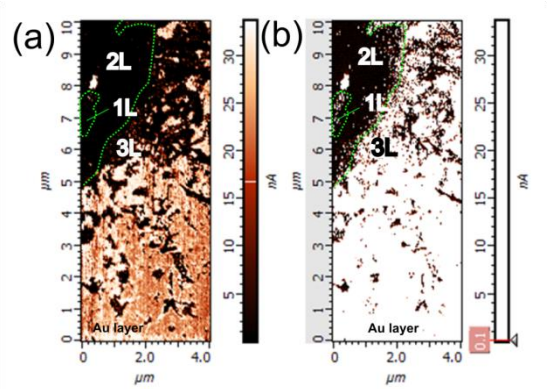

The electrical conductivity of flakes was measured by conductive AFM. The sample preparation can be found in the supplementary material Figure S6. The topography image is shown in Figure S7. Figure 6 (a) and (b) are the same current distribution map with different current scales, in which Figure 6 (b) is able to show low current value. The boundaries of 2D monolayers 2L and 3L are marked with green dash line, based on the current level. We can see monolayer 2L is less conductive than monolayer 3L. Therefore, the interfaces might block the flow of current. It probably influences the conductivity of overall crystalline thin film.

The reason of layer formation is still not fully clear. In general, we assume the layers in amorphous films could be formed due to the compositional derivation. And the compositional derivation is possibly caused by the fast cooling of material. Specifically, when the vapor of GST condenses on the cold substrate, it might forms a liquid thin film. As the temperature difference between the thin film and substrate, it tends to form a temperature gradient. Therefore, the composition variation occurs under different temperature. We have not found any way to avoid the layers formation. However, there are still issues waiting to be solved.

Conclusions

In this paper, we address sputtered GST thin film owns a multiple 2D monolayers. More importantly, the AFM determines the thickness of the crystalline GST flakes, which is 10 nm. However, the knowledge of 2D monolayer formation is still limited. We still do not understand how to avoid the 2D monolayers formation. Although the appearance of thin film is compact and uniform, the layers can be separated from the thin film. The next step is towards to answer questions above. Whether thin film without 2D monolayers could be prepared by other technique as a flash thermal evaporation or pulsed laser deposition is still waiting to be explored. However, if 2D layers formation is the result of fast cooling of material, any methods based on the high temperature are less likely successful. In this situation, molecular beam epitaxy is worth to try.

Experiments

The GST thin film was deposited to silicon wafer via magnetron sputtering, where the power in 10W and the duration of sputtering is 1 hour. The Van der Pauw was measured from ambient temperature to 380℃ in 2℃/min. The similar method was also applied to the amorphous GST thin film from ambient temperature to 270℃ in 2℃/min, in order to get crystalline GST thin film. Then the crystalline GST thin film was exfoliated via acetone. The acetone is in volatile and low surface tension. Therefore, it is easy to flow in between the 2D monolayers and the vapor from acetone results in the exfoliation of crystalline 2D monolayers (referred as crystalline flakes). The flakes dispersed in acetone were transferred to a sputtered W thin film for further observation. The remaining acetone solution is dried in a vacuum environment. The similar exfoliation was also applied to the amorphous thin film, in order to get amorphous flakes. SEM (scanning electron microscope) images were taken from JEOL 7500 at 5kV acceleration voltage. The AFM images were taken by AFM Solver Pro M, NT-MDT in semi-contact mode. The TEM images were taken on microscope JEOL JEM 3010 TEM.

Conflicts of interest

In accordance with our policy on Conflicts of interest please ensure that a conflicts of interest statement is included in your manuscript here. Please note that this statement is required for all submitted manuscripts. If no conflicts exist, please state that “There are no conflicts to declare”.

Acknowledgements

The authors thank for financial support from the grant of the Ministry of Education, Youth and Sports of Czech Republic (grant LM2015082), the European Regional Development Fund-Project "Modernization and upgrade of the CEMNAT" (No. CZ.02.1.01/0.0/0.0/16_013/0001829), and the project of Czech Grant Agency (GA CR) 19-20792S.

Notes and references

1 Micron and Intel Produce Breakthrough Memory Technology, https://www.micron.com/about/news-and-events/media-relations/media-kits/3d-xpoint-technology.

2 M. Wuttig and N. Yamada, *Nat. Mater.*, 2007, **6**, 824–832.

3 B. Casarin, A. Caretta, B. Chen, B. J. Kooi, R. Ciprian, F. Parmigiani and M. Malvestuto, *Nanoscale*, 2018, **10**, 16574–16580.

4 D. Lencer and M. Wuttig, *NATO Sci. Peace Secur. Ser. B Phys. Biophys.*, 2009, 413–428.

5 S. R. Ovshinsky, *Phys. Rev. Lett.*, 1968, **21**, 1450–1453.

6 J. Feinleib, J. Deneufville, S. C. Moss and S. R. Ovshinsky, *Appl. Phys. Lett.*, 1971, **18**, 254–257.

7 D. J. Wouters, R. Waser and M. Wuttig, *Proc. IEEE*, 2015, 103, 1274–1288.

8 N. Yamada, E. Ohno, K. Nishiuchi, N. Akahira and M. Takao, *J. Appl. Phys.*, 1991, **69**, 2849–2856.

9 T. Nishihara, A. Tsuchino, Y. Tomekawa, H. Kusada, R. Kojima and N. Yamada, *Jpn. J. Appl. Phys.*, 2011, **50**, 62503.

10 M. H. Jang, S. J. Park, S. J. Park, M. H. Cho, E. Z. Kurmaev, L. D. Finkelstein and G. S. Chang, *Appl. Phys. Lett.*, 2010, **97**, 15211.

11 J. Hegedüs and S. R. Elliott, *Nat. Mater.*, 2008, **7**, 399–405.

12 M. S. Youm, Y. T. Kim and M. Y. Sung, *Appl. Phys. Lett.*, , DOI:10.1063/1.2773758.

13 T. Kato and K. Tanaka, *Japanese J. Appl. Physics, Part 1 Regul. Pap. Short Notes Rev. Pap.*, 2005, **44**, 7340–7344.

14 H. Nakamura, I. Rungger, S. Sanvito, N. Inoue, J. Tominaga and Y. Asai, *Nanoscale*, 2017, **9**, 9386–9395.

15 U. Russo, D. Ielmini, A. Redaelli and A. L. Lacaita, *IEEE Trans. Electron Devices*, 2006, **53**, 3032–3039.

16 S. Lim, S. Lee, J. Woo, D. Lee, J. Park, J. Song, K. Moon, J. Park, A. Prakash and H. Hwang, in *2014 14th Annual Non-Volatile Memory Technology Symposium, NVMTS 2014*, 2015.

17 P. Marvan, V. Mazánek and Z. Sofer, *Nanoscale*, 2019, **11**, 4310–4317.

18 J. Xia, J. Yan and Z. X. Shen, *FlatChem*, 2017, 4, 1–19.

19 S. M. Tan, Z. Sofer, J. Luxa and M. Pumera, *ACS Catal.*, 2016, **6**, 4594–4607.

20 J. Xia, J. Wang, D. Chao, Z. Chen, Z. Liu, J. L. Kuo, J. Yan and Z. X. Shen, *Nanoscale*, 2017, **9**, 7533–7540.

21 M. Zhu, K. Ren, L. Liu, S. Lv, X. Miao, M. Xu and Z. Song, *Phys. Rev. Mater.*, 2019, **3**, 033603.

22 G. Wang, A. Lotnyk, Q. Nie, R. Wang, X. Shen and Y. Lu, *Langmuir*, 2018, **34**, 15143–15149.

23 A. Lotnyk, T. Dankwort, I. Hilmi, L. Kienle and B. Rauschenbach, *Nanoscale*, 2019, 10838–10845.

24 J. Momand, R. Wang, J. E. Boschker, M. A. Verheijen, R. Calarco and B. J. Kooi, *Nanoscale*, 2017, **9**, 8774–8780.